

Article

Structural and Biochemical Characterization of a Cyanobacterial PP2C Phosphatase Reveals Insights into Catalytic Mechanism and Substrate Recognition

Yunlong Si, Ye Yuan, Yue Wang, Jin Gao, Yanbo Hu, Shiqiong Feng and Jiyong Su *

School of Life Sciences, Northeast Normal University, Changchun 130024, China; siy1071@nenu.edu.cn (Y.S.); yuany268@nenu.edu.cn (Y.Y.); wangy147@nenu.edu.cn (Y.W.); gaoj466@nenu.edu.cn (J.G.); huyb705@nenu.edu.cn (Y.H.); fengsq104@nenu.edu.cn (S.F.)

* Correspondence: sujy100@nenu.edu.cn; Tel.: +86-132-4431-8851

Academic Editor: David D. Boehr

Received: 26 February 2016; Accepted: 20 April 2016; Published: 26 April 2016

Abstract: PP2C-type phosphatases play roles in signal transduction pathways related to abiotic stress. The cyanobacterial PP2C-type phosphatase tPphA specifically dephosphorylates the PII protein, which is a key regulator in cyanobacteria adapting to nitrogen-deficient environments. Previous studies have shown that residue His39 of tPphA is critical for the enzyme's recognition of the PII protein; however, the manner in which this residue determines tPphA substrate specificity is unknown. Here, we solved the crystal structure of H39A, a tPphA variant. The structure revealed that the mutation of residue His39 to alanine changes the conformation and the flexibility of the loop in which residue His39 is located, and these changes affect the substrate specificity of tPphA. Moreover, previous studies have assumed that the FLAP subdomain and the third metal (M3) of tPphA could mutually influence each other to regulate PP2C catalytic activity and substrate specificity. However, despite the variable conformations adopted by the FLAP subdomain, the position of M3 was consistent in the tPphA structure. These results indicate that the FLAP subdomain does not influence M3 and *vice versa*. In addition, a small screen of tPphA inhibitors was performed. Sanguinarine and Ni²⁺ were found to be the most effective inhibitors among the assayed chemicals. Finally, the dimeric form of tPphA was stabilized by cross-linkers and still exhibited catalytic activity towards *p*-nitrophenyl phosphate.

Keywords: PP2C variant crystal structure; PP2C inhibitor; protein chemical cross-linking; biological metal

1. Introduction

PP2C-type phosphatases (PP2Cs) are widely distributed in eukaryotes and prokaryotes and participate in many signaling pathways, especially during responses to abiotic stress. Wip1, a mammalian PP2C, is induced in a p53-dependent manner in response to ionizing radiation [1]. In plants, a large group of PP2Cs regulate responses to abiotic stresses, including drought, cold, and salinity [2]. Yeast PP2Cs are involved in responses to osmotic stress [3]. The cyanobacterial PP2C known as PphA/tPphA was identified to specifically dephosphorylate the PII protein, which acts as a key regulator in cyanobacteria adapting to nitrogen-deficient environments [4].

In our previous research, we performed alanine-scanning mutagenesis of tPphA to study how tPphA specifically recognizes the PII protein [5]. As a complement to this mutagenesis, enzymatic assays were performed. A variant of tPphA, H39A, could not dephosphorylate the PII protein but exhibited activity towards *p*-nitrophenyl phosphate (*p*NPP) and phospho-peptides [5]. These results indicated that His39 is critical for recognizing the PII protein. However, there is a lack of structural information to explain the effect of the mutation of His39 to alanine in tPphA. Moreover, His39 is close

to the catalytic center of tPphA, and whether the mutation affects this catalytic center is unknown. Therefore, solving the crystal structure of H39A should provide interesting insights. Furthermore, by comparing the structure of the wild-type tPphA enzyme structure to the mutant H39A structure, new clues into how tPphA recognizes substrates may be obtained.

The crystal structures of plant and prokaryotic PP2Cs show the presence of three divalent cations (M1, M2, and M3) in the catalytic centers of these proteins [6–11]. We previously demonstrated that all of these divalent cations are essential for PP2C activity [12]. M3 is close to a long and flexible loop known as the FLAP subdomain. It was assumed that M3 and FLAP can influence each other's positions to regulate PP2C catalytic activity and substrate specificity [7,8]. Therefore, solving the structure of an active PP2C variant and comparing its M3 and FLAP subdomain positions against those in wild-type PP2C structures should prove a worthwhile endeavor. Because the H39A variant can dephosphorylate substrates, the structure of H39A should prove to be a good candidate for explaining the relationship that exists between M3 and FLAP.

PP2C inhibitor research has been focused mainly on Wip1 [2,13] because the overexpression of Wip1 is believed to promote tumorigenesis by inactivating the tumor-suppressor functions of multiple substrates [14–17]. However, there is still a lack of effective inhibitors for other PP2Cs. PP2Cs dephosphorylate substrates via a S_N2 mechanism [12]. They require Mg^{2+}/Mn^{2+} as ligands, which activate a nucleophilic hydroxide ion to attack phosphate groups on their substrates. Subsequently, the phosphate groups are hydrolyzed from the substrates. To inhibit this S_N2 reaction, variable divalent cations, divalent cation chelators, chemical mimics of nucleophilic hydroxides, chemical mimics of phosphate transition states, and chemical mimics of substrates can be used. Comparing the inhibitory effects of these chemicals on PP2Cs could provide useful information to aid in the design of effective PP2C inhibitors.

The crystal-packing contacts of tPphAs [11] imply that this enzyme may form a homodimer through its FLAP subdomain. To stabilize this dimeric tPphA, chemical cross-linkers could be used. Moreover, whether cross-linked tPphA retains catalytic activity is worth determining.

In this report, the structures of wild-type tPphA and H39A were solved, and the inhibitory effects of several chemicals on tPphA were assayed. The dimeric form of tPphA was characterized, and this complex showed activity towards pNPP.

2. Results and Discussion

2.1. His39 Determines tPphA Substrate Specificity

Wild-type tPphA and H39A were crystallized under previously described conditions [11]. The crystal structure parameters are listed in Table 1. The overall structures were similar to published tPphA structures [12]. However, there were variations in all of the structures, especially in the region housing the FLAP domain (Thr138 → Leu163) and loops connecting α helices and β strands (Figure 1A).

The loop (Gly₃₇ → Gly₄₂) connecting β_3 and α_1 , which contains His39, was disordered in three of the tPphA structures (PDB codes: 2J82, 2XZV and 5ITI). However, the structure of this loop in the H39A structure (PDB code: 5D2U) could be determined (Figure 1B). These results indicate that the mutation of His39 to alanine made the loop more rigid than the corresponding loop in wild-type tPphA. Moreover, H39A exhibited a different conformation than D119A (Figure 1B). Overall, the different conformation and flexibility of this loop in H39A compared to the wild-type enzyme may underlie the change in the substrate specificity of H39A. This relationship could explain our previous enzymatic assay results in which H39A could not recognize the natural substrate of tPphA, *i.e.*, the PII protein [5].

In the plant PP2Cs ABI1 and HAB1, there is a glycine residue at the position equivalent to tPphA His39, in the loop connecting β_3 and α_1 [6,18]. The mutation of this glycine to aspartate inhibited the abilities of ABI1 and HAB1 to dephosphorylate casein but did not greatly affect the abilities of these two

phosphatases to dephosphorylate their other physiological substrates [19–22]. These results indicate that this glycine residue in plant PP2Cs also plays a role in helping phosphatases recognize substrates.

Table 1. Crystallographic data collection and refinement statistics ^a.

Parameters	PDB Number	
	5D2U	5ITI
Wavelength (Å)	0.9794	0.9794
Resolution (Å)	19.23–1.8 (1.84–1.8)	19.23–1.95 (2.0–1.95)
Space group	C222 ₁	C222 ₁
Unit cell parameters (a, b, c) (Å)	38.04 153.87 82.76	38.01 153.82 82.93
No. of measured reflections	144931 (8901)	116108 (8160)
No. of unique reflections	23018 (1344)	18220 (1267)
Completeness (%)	99.9 (100.0)	99.9 (100.0)
Multiplicity	6.3 (6.6)	6.4 (6.3)
R _{merge} (%) ^b	7.0 (97.1)	6.3 (79.6)
R _{pim} (%) ^c	3.2 (43.0)	2.9 (36.6)
<I/σ(I)>	14.4 (2.1)	15.7 (2.5)
Refine		
Resolution limits (Å)	19.23–1.8	19.23–1.95
R _{model} (%) ^d	21.3	21.5
R _{free} (%) ^e	24.8	26.8
No. of waters	112	87
Rmsd bond lengths (Å)	0.0085	0.0077
Rmsd bond angles (°)	1.335	0.958
Average B factors, all atoms (Å ²)	37.0	40.9
B factor of metal ions: M1/M2/M3	31.8/28.9/42.7	32.85/32.18/48.72
Ramachandran plot ^f residues in favored regions (%)	93.48	93.9
Ramachandran outliers (%)	0	0

^a The values in parentheses correspond to the shell with the highest resolution. ^b $R_{\text{merge}} = \sum_{hkl} \sum_i |I(hkl)_i - \langle I(hkl) \rangle| / \sum_{hkl} \sum_i I(hkl)_i$. ^c $R_{\text{pim}} = \sum_{hkl} |F_o(hkl) - F_c(hkl)| / \sum_{hkl} |F_o(hkl)|$, where F_o and F_c are the observed and calculated structure factors, respectively. ^d $R_{\text{model}} = \sum_{hkl} |F_o(hkl) - F_c(hkl)| / \sum_{hkl} |F_o(hkl)|$, where F_o and F_c are the observed and calculated structure factors, respectively. ^e A 5% random test set. ^f Calculated using MolProbity.

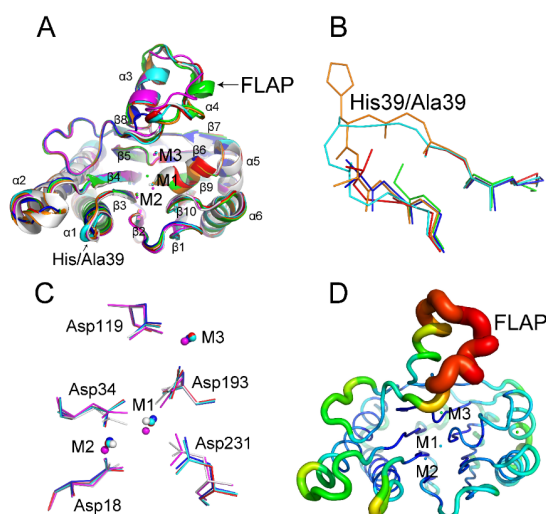


Figure 1. Analysis of tPphA structures (H39A: cyan, PDB: 5D2U. tPphA: blue, PDB: 2J82; white, PDB: 2J86_A; magenta, PDB: 2J86_B; red, PDB: 5ITI. D119A: orange, PDB: 2XZV. D193A: green, PDB: 2Y09). **(A)** The H39A structure is merged with the structures of wild-type tPphA and the D119A and D193A variants. His/Ala 39 is located within a loop that is across from the FLAP subdomain. The FLAP domain adopts different conformations in different tPphA structures. **(B)** The loops in which His39/Ala39 are located in different structures are merged with each other. The conformation of this loop in the H39A structure is different from those in the other tPphA structures. **(C)** The catalytic center of H39A was merged with the catalytic cores of other wild-type tPphAs. The positions of the three divalent cations within these catalytic centers are identical. The positions and conformations of five conserved aspartate residues in the H39A structure are the same as those in two other tPphA structures (PDB: 2J82 and 5ITI), but different from those in two monomers in a third tPphA structure (PDB: 2J86). **(D)** The colors used in the figure indicate the B factor values for H39A (blue < green < orange < red). The B factor value of the FLAP subdomain is very high, which indicates that this region is very flexible.

2.2. New Insights into the Catalytic Center of tPphA

Three calcium ions were identified in each of the catalytic centers of the two tPphA structures solved here. This ion composition is different from that found in previously published tPphA structures [11,12]. In one published tPphA crystal structure (PDB: 2J86), three magnesium ions were identified in the catalytic center. This structure was solved from a crystal grown in 0.2 M CaCl₂, and the crystal was soaked with pNPP and 0.2 M MgCl₂ prior to diffraction. In another tPphA structure (PDB: 2J82), one fully occupied magnesium ion (M3) was present from the purification procedure used, one fully occupied calcium ion (M2) was present from the crystallization conditions used, and one metal ion (M1) was present that comprised a mixture of magnesium and calcium. Although the ion compositions of the different structures varied, the positions of the three divalent cations in the tPphA structures were nearly identical (Figure 1C). The mutual distance of the same divalent cations in different tPphA structures was less than 0.5 Å.

Five conserved aspartate residues present in the structures of all high-resolution tPphA structures (better than 2.0 Å) were merged with each other (Figure 1C). Both tPphA structures solved here and a 1.28 Å tPphA structure (PDB: 2J82) were generated from crystals grown under the same conditions. The positions of the five aspartate residues in these three structures were found to be nearly identical (all-atom RMSD value: 0.25). By contrast, the positions of these aspartate residues in wild-type tPphA (PDB: 2J82 and 5ITI) and H39A structures showed differences (all-atom RMSD values: 0.86, 0.81, 0.73, and 0.98) compared to the aspartate residues in another structure (PDB: 2J86) that contains two tPphA subunits in the asymmetric unit. In the 2J86 structure, three Mg²⁺ are present in the catalytic center. The crystal used to generate this structure was soaked with pNPP and 0.2 M MgCl₂ prior to diffraction. These results imply that the catalytic center of the 2J86 structure may be in an “active state”, whereas the tPphA structures bound with Ca²⁺ may be in an “inhibited state”. Ca²⁺ and Mg²⁺ have different geometries, and Ca²⁺ is larger than Mg²⁺. Mg²⁺ serves as a ligand of tPphA, whereas Ca²⁺ serves as an inhibitor of tPphA (See 2.4). When tPphA is complexed with Mg²⁺, Mg²⁺ may induce aspartate residues at suitable positions of tPphA to adopt conformations that enable the enzyme to dephosphorylate substrates. By contrast, if tPphA is coordinated with Ca²⁺, then Ca²⁺ may force the aspartate residues to adopt conformations that prevent tPphA from dephosphorylating its substrates. Therefore, Ca²⁺ may inhibit the catalytic activity of tPphA not only because of its unique characteristics (size and geometry) but also by slightly changing the structure of the catalytic center.

2.3. Relationship between the FLAP Subdomain and M3

The most flexible region of tPphA is the FLAP subdomain. The FLAP subdomain shows variable conformations in different tPphA structures (Figure 1A). The RMSD values between parts of FLAP subdomains (Ile151 → Leu163) are listed in Table 2. Most of the RMSD values are higher than 1. Two exceptions are the RMSD values (0.681 and 0.707) between two tPphA structures solved here and between D119A and D193A. Although these RMSD values are lower than other RMSD values, they are nonetheless high. The structure of most of the FLAP subdomain in one tPphA structure (PDB: 2J82) could not be determined. Therefore, the RMSD values of this FLAP domain relative to other FLAP domains could not be determined. The bottom of the FLAP subdomain in this tPphA structure (PDB: 2J82) is visible, and this region adopts a significantly different conformation compared to those found in other tPphA structures (Figure 1A). In addition, the B factor of the FLAP subdomain is significantly higher than those in other parts of tPphA (Figure 1D). Overall, these results indicate that the FLAP subdomain is a flexible region of tPphA.

Asp119 and Asp193 are the only two residues found to coordinate with M3. The mutation of Asp119 and Asp193 to alanine caused tPphA to lose catalytic activity. The crystal structures of D119A and D193A only show M1 and M2 in the catalytic center. This result indicates that M3 is essential for the dephosphorylation reaction catalyzed by tPphA [12]. It has been suggested that the FLAP subdomain and M3 can influence each other's positions and regulate PP2C catalytic activity and substrate specificity [7,8,10]. Here, the FLAP subdomain showed variable conformations in

different structures, while the mutual distance of M3 in different tPphA structures was less than 1 Å. (Figure 1A,C). Moreover, in a previous study, His161 of the FLAP subdomain, a residue that is located within the vicinity of the catalytic core and occupies the same position of Ser160 of *M. tuberculosis* PstP [7], was replaced with either serine or alanine. However, the mutation of His161 only slightly affected tPphA activity. This result indicates that the FLAP subdomain does not influence the position or function of M3 and *vice versa*. Overall, the FLAP subdomain and M3 are independent of each other.

Table 2. C α RMSD values of a portion of the FLAP subdomain (Ile151 \rightarrow Leu163).

C α RMSD	Wt-tPphA PDB: 2J86_A	Wt-tPphA PDB: 2J86_B	Wt-tPphA PDB: 5ITI	H39A PDB: 5D2U	D119A PDB: 2XZV	D193A PDB: 2Y09
Wt-tPphA PDB: 2J86_A	-	2.223	2.858	2.928	3.343	2.449
Wt-tPphA PDB: 2J86_B	2.223	-	2.244	2.199	2.734	1.635
Wt-tPphA PDB: 5ITI	2.858	2.244	-	0.681	1.844	1.084
H39A PDB: 5D2U	2.928	2.199	0.681	-	1.802	1.215
D119A PDB: 2XZV	3.343	2.734	1.844	1.802	-	0.707
D193A PDB: 2Y09	2.449	1.635	1.084	1.215	0.707	-

2.4. Inhibition Effects of Nine Chemicals on tPphA Activity

The catalytic constants of tPphA and H39A towards casein were determined (Table 3). The K_m and K_{cat} of H39A towards casein are higher than those of tPphA. However, the K_{cat}/K_m of H39A is almost equivalent to the wild-type enzyme. This result indicates that the H39A variant has the same catalytic efficiency as tPphA.

Table 3. Catalytic constants of tPphA and H39A towards casein.

Enzyme Variants	K_m (μ M)	K_{cat} (s^{-1})	K_{cat}/K_m (s^{-1}/M)
tPphA	0.85 ± 0.16	1.12 ± 0.26	$1.36 \times 10^6 \pm 0.31 \times 10^6$
H39A	1.23 ± 0.20	1.69 ± 0.11	$1.37 \times 10^6 \pm 0.09 \times 10^6$

A small screen of tPphA inhibitors was performed. Nine chemicals were used to inhibit tPphA activity. The inhibitory mechanisms of these chemicals on tPphA were different. By comparing the inhibitory effects of these chemicals on tPphA, a better inhibitory mechanism could potentially be identified, and a new effective inhibitor could be designed based on this information.

We previously showed that H39A does not dephosphorylate the PII protein because this variant could not recognize it. Therefore, a substitute protein, casein, was used in this assay. Casein has been used in many PP2C studies [19–23]. We found that H39A could dephosphorylate this protein. Therefore, we used casein as a substitute for the PII protein to investigate the inhibitory effects of different chemicals on H39A. The IC₅₀s of nine chemicals on tPphA and H39A with regard to the dephosphorylation of *p*NPP and casein were determined (Figure 2 and Table 4).

Preliminary pre-clinical *in vitro* and *in vivo* studies have demonstrated that sanguinarine causes apoptosis in human cancer cells [24–29]. Recently, sanguinarine was identified as inhibiting the dephosphorylation of casein by human PP2C α with an IC₅₀ value of 2.5 μ M [23], although the inhibitory mechanism is unknown. Here, sanguinarine also showed good inhibition of tPphA (Table 4). The IC₅₀ value of sanguinarine on tPphA with regard to the dephosphorylation of casein was approximately 30 times higher than that obtained for PP2C α . However, the IC₅₀ value of sanguinarine on tPphA with regard to the dephosphorylation of *p*NPP was only four times higher than that obtained for PP2C α . These results imply that the structural differences between PP2C α and tPphA may cause sanguinarine to produce different inhibitory effects on these enzymes. Future work should be focused on explaining how this compound inhibits PP2Cs, as well as how chemical modifications of this compound may improve its specific inhibitory effect on PP2Cs.

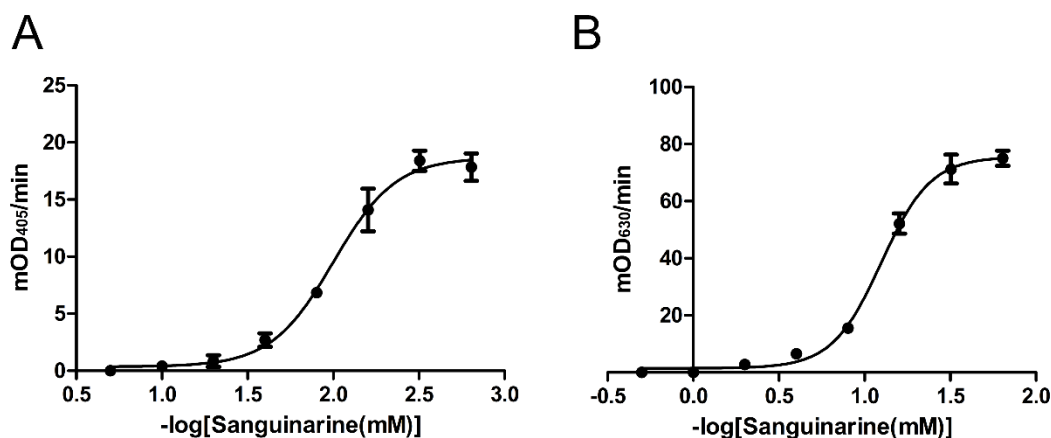


Figure 2. IC₅₀s of sanguinarine on wild-type tPphA with regard to the dephosphorylation of *p*NPP and casein. The IC₅₀s of other chemicals on wild-type tPphA and H39A were measured in triplicate. The values are listed in Table 4.

Table 4. IC₅₀s of nine compounds on tPphA with regard to the dephosphorylation of *p*NPP and casein.

IC ₅₀ (mM)	<i>p</i> NPP Assay		Casein Assay	
	tPphA	H39A	tPphA	H39A
Sanguinarine	0.010 ± 0.002	0.008 ± 0.001	0.08 ± 0.03	0.07 ± 0.02
NiSO ₄	0.04 ± 0.01	0.08 ± 0.02	0.21 ± 0.02	0.15 ± 0.01
CaCl ₂	17.66 ± 1.57	10.69 ± 1.64	19.48 ± 3.86	11.86 ± 4.26
MgCl ₂	10.98 ± 1.11	9.64 ± 0.93	-	-
EDTA	0.93 ± 0.05	1.21 ± 0.06	2.29 ± 0.09	2.50 ± 0.18
NaF	21.08 ± 3.58	23.73 ± 2.59	1.24 ± 0.15	32.52 ± 3.84
AlF ₃	67.52 ± 5.69	156.34 ± 5.23	76.49 ± 2.69	63.32 ± 5.93
Sodium phenyl phosphate	8.65 ± 1.31	7.37 ± 1.58	-	-
Glycerol-phosphate	17.18 ± 0.83	25.93 ± 3.60	12.36 ± 2.65	4.52 ± 1.89

The replacement of Mn²⁺ in the catalytic center of tPphA with two divalent cations (Ni²⁺ and Ca²⁺) could also inhibit tPphA activity. The low IC₅₀ value of Ni²⁺ measured in this report suggests that this divalent cation is a stronger inhibitor of tPphA than Ca²⁺, which also shows inhibitory effects on other PP2Cs [30–36]. Other divalent cations have also been reported to inhibit PP2C catalytic activity [32,34,37]. The inhibitory effects of these divalent cations on PP2Cs may come from the replacement of Mg²⁺/Mn²⁺ with the above ions. It is assumed that the different sizes and preferred geometries of Mg²⁺/Mn²⁺ vs. these divalent cations are responsible for the loss of activity in PP2C [38].

Several inhibitors of Wip1 have previously been synthesized [13,14]. These inhibitors specifically inhibit Wip1 by binding to the FLAP subdomain. Because the FLAP subdomain helps PP2Cs recognize their specific substrates, its primary and tertiary structures should be considered in the design of new inhibitors. Based on the present results, a good strategy for the design of PP2C inhibitors is the creation of compounds which contain both divalent cation moieties and other moieties that could specifically bind to the FLAP subdomain: first, the FLAP subdomain interaction moieties bind to the unique FLAP subdomain of PP2C; second, divalent cation moieties disturb the catalytic center of PP2C and inhibit its activity.

In previous studies, we showed that Mg²⁺ could activate tPphA to dephosphorylate the PII protein and other phosphopeptides but could not induce tPphA to dephosphorylate *p*NPP [5]. This characteristic of Mg²⁺ has also been observed in other *p*NPP assays of PP2Cs [34,39]. The IC₅₀ values

of Mg^{2+} on tPphA and H39A when *p*NPP was used as substrate were determined as 10.98 and 9.64 mM, respectively.

EDTA, NaF and AlF_3 are general inhibitors of phosphatase. EDTA effectively chelates divalent cations from proteins. The IC₅₀s of EDTA on tPphA with regards to the dephosphorylation of *p*NPP and casein are 0.93 and 2.29 mM, respectively. PP2Cs dephosphorylate substrates via an S_N2 mechanism. A nucleophilic hydroxide ion activated by M1 and M2 is essential for the dephosphorylation reaction [12]. F^- mimics the nucleophilic hydroxide ions present in phosphatase active sites [40]; therefore, F^- could be used as an inhibitor of tPphA. The IC₅₀ value of NaF on tPphA with regard to the dephosphorylation of casein is 1.24 mM, which is much lower than the value obtained for H39A. Thus, the histidine at position 39 may help tPphA correctly place a substrate so that hydroxide ions cannot easily diffuse into the catalytic center of the enzyme; in this case, a low concentration of NaF would be sufficient to inhibit 50% of tPphA's activity. By contrast, the substitution of His39 with an alanine may alter the contact points that form between tPphA and casein such that hydroxide ions could easily reach the catalytic center; in this case, a high concentration of NaF would be needed to reduce H39A activity. Indeed, NaF concentrations of 21.08 mM and 23.73 mM are required to reduce 50% of tPphA and H39A's activities, respectively, when using *p*NPP as a substrate. AlF_3 structurally mimics the transition state of phosphate. It is assumed that phosphate groups on a given substrate can be replaced with AlF_3 , which will inhibit dephosphorylation reactions [41]. However, AlF_3 could not effectively inhibit tPphA's dephosphorylation of its substrates.

Sodium phenyl phosphate, a compound structurally related to *p*NPP, could not be dephosphorylated by tPphA (according to a malachite green assay). The main difference between sodium phenyl phosphate and *p*NPP is that sodium phenyl phosphate lacks one nitro group. This indicates that the nitro group of *p*NPP is required for tPphA to dephosphorylate *p*NPP. Sodium phenyl phosphate could inhibit tPphA dephosphorylation of *p*NPP. In addition, glycerol-phosphate, which has three phosphate groups, showed some inhibition of tPphA activity.

2.5. An Active tPphA Dimer

In tPphA structures, one single tPphA molecule forms an asymmetric unit. The FLAP subdomain of a tPphA molecule in one asymmetric unit forms an interaction with the FLAP subdomain of a tPphA molecule in another asymmetric unit via crystal-packing contact (Figure 3A). However, tPphA only showed one single peak on size exclusion chromatography [5]. This result indicates that tPphA can also exist in a monomeric form. Thus, to stabilize the tPphA dimer, two chemicals (glutaraldehyde and DTSSP) were used to cross-link tPphA. Glutaraldehyde is a classic cross-linker for the immobilization of enzymes and can be used in many types of medium [42]. DTSSP has dual *N*-hydroxysulfosuccinimide esters that can react with primary amines on proteins. A disulfide bond present in the center of DTSSP can be cleaved with reducing agents. The dimeric form of tPphA was stabilized by cross-linking with glutaraldehyde and DTSSP (Figure 3B,C). The tPphA dimer cross-linked by glutaraldehyde was a stable dimer: neither SDS nor DTT could destroy this complex (Figure 3B). By contrast, the tPphA dimer that was cross-linked by DTSSP could be decomposed by DTT (Figure 3C).

After the glutaraldehyde cross-linking reaction, tPphA monomers and dimers were separated over a gel filtration column. There were two main peaks in following size exclusion chromatography (Figure 3D): A 15 mL peak that mainly contained dimeric tPphA and an 18 mL peak that mainly contained monomeric tPphA. The activities of the protein fractions collected from the gel filtration were assayed using *p*NPP as a substrate. After cross-linking, both tPphA monomers and tPphA dimers could dephosphorylate *p*NPP (Figure 3D).

tPphA is highly soluble and easy to purify. It also maintains reaction activity at 65 °C [11]. Even when crosslinked by glutaraldehyde, tPphA still maintains activity. These characteristics of tPphA may allow it to be immobilized on several media through glutaraldehyde crosslinking and it is used in the chemical industry for dephosphorylating particular compounds under high temperature

conditions. In addition, because tPphA is inhibited by several divalent cations, such as Ni^{2+} , it can also be immobilized in a biosensor to detect divalent cations.

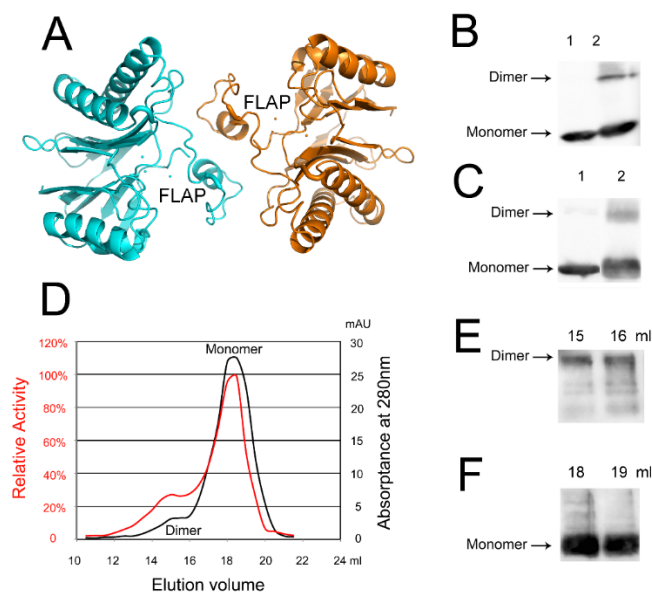


Figure 3. (A) Crystal-packing contacts in tPphA structures (PDB: 2J82, 2XZV, 2Y09, 5D2U, and 5ITI) are similar and imply a dimer. For example, in the H39A structure, each H39A molecule forms an asymmetric unit. Two H39A molecules could pack with each other through the FLAP subdomain. (B) tPphA cross-linked by glutaraldehyde. A dimer of tPphA is stabilized by glutaraldehyde (the upper band in Lane 2). (C) tPphA cross-linked by DTSSP. The conditions in Lane 1 and Lane 2 are the same, except that the tPphA dimer in Lane 1 was decomposed using DTT. There is less tPphA dimer in Lane 1 than in Lane 2. (D) tPphA cross-linking products were separated by gel filtration. The activities of the protein fractions were determined by pNPP assay. The cross-linked dimer of tPphA could still dephosphorylate pNPP. (E,F) Western blotting. Fractions (15, 16, 18, and 19 mL) from (D) were analyzed by Western blotting.

3. Experimental Section

3.1. Overexpression and Purification of PP2C Phosphatases

tPphA and H39A were expressed and purified as previously described [5,12] with some modifications. For overexpression of the recombinant proteins, the constructs were transformed into *E. coli* BL21 (DE3) cells and grown in LB medium supplemented with ampicillin (100 $\mu\text{g}/\text{mL}$). When the optical density (O.D. 600) of the cultures reached 0.6–0.8, IPTG was added to a final concentration of 0.5 mM to induce protein overproduction. After a 16 h induction at 25 $^{\circ}\text{C}$, the cells were harvested by centrifugation and lysed by sonication on ice in lysis buffer. The protein lysis buffer consisted of 50 mM Tris-HCl, pH 8.0; 300 mM NaCl; 20 mM imidazole; and 2 mM MgCl_2 . The lysates were centrifuged for 30 min at 14,000 g. The clarified cell extracts were used for protein purification. Ni-NTA Agarose (Qiagen, Hilden, Germany) was used to purify His-tagged proteins.

After purification, all his-tagged proteins were dialyzed in 10 mM Tris-HCl, pH 7.0; 150 mM NaCl; 50 mM KCl; 3 mM DTT; 0.5 mM EDTA; 5 mM MgCl_2 , and 50% glycerol (*v/v*). The proteins were then stored at -80°C and used for enzymatic assays. For H39A crystallization, each 1 mg of His-tagged protein was digested with 10 units (NIH unit) thrombin to remove the $6 \times$ His tag. At the same time, H39A was dialyzed in 10 mM Tris-HCl, pH 7.0; 150 mM NaCl; 50 mM KCl; and 5 mM MgCl_2 . After the digestion, a short peptide (Gly-Ser-His) remained at the N-terminal end of H39A. The digestion solution was loaded onto a desalting column (Sephadex G10, GE) for buffer exchange. The desalting buffer was composed of 10 mM Tris-HCl, pH 7.0; 150 mM NaCl; 50 mM KCl; 3 mM DTT; and

0.5 mM EDTA. Finally, H39A was concentrated to 45 mg/mL using an Amicon Ultra-15 Centrifugal Filter (10 kDa cut-off, Billerica, USA) and stored at -80°C . The purity of H39A was $>90\%$ according to SDS-PAGE.

3.2. H39A Crystallization, X-ray Data Collection and Structure Determination

Wild-type tPphA and H39A were crystallized as previously described [11]. Crystals of wild-type tPphA and H39A (typical size of $0.2 \times 0.2 \times 0.05$ mm) were grown using the hanging drop vapor diffusion method from drops containing 1 μL of protein (45 mg/mL) and 1 μL of solution from the well, which was composed of 100 mM Tris-HCl, pH 7.4; 200 mM CaCl_2 ; and 26% PEG3350 (*v/v*). Before data collection, the crystals were soaked into a reservoir solution supplemented with 20% (*v/v*) glycerol as cryoprotectant for 1 min and then flash-frozen in liquid nitrogen. Data sets were collected from the crystals at 100 K at Shanghai Synchrotron Radiation Facility (Shanghai, China).

The data sets were indexed and integrated using XDS [43] and scaled using Aimless [44] from the CCP4 package (6.4.0, Science and Technology Facilities Council, Rutherford Appleton Laboratory, Didcot, Oxon, UK, 2015) [45]. Structures were determined by Phaser [46] with a molecular replacement method using the structure of tPphA variant D193A (PDB: 2XZV) as the search model. Structure refinement and water updating were performed using Phenix [47] refine and manual adjustment. Final structure validations were performed using MolProbity [48,49]. All structure figures were generated using PyMOL [50] or Coot [51].

3.3. pNPP Assay

The half-maximal inhibitory concentrations (IC_{50}) of nine chemicals (sanguinarine, NiSO_4 , EDTA, NaF_3 , AlF_3 , CaCl_2 , MgCl_2 , glycerol-phosphate, and sodium phenyl phosphate) on PP2C phosphatase with regard to the dephosphorylation of pNPP were determined. Standard assays were performed in a volume of 200 μL containing 0.2 μg phosphatases in a buffer consisting of 10 mM Tris-Cl, pH 8.5; 50 mM NaCl; 1 mM DTT; and 2 mM MnCl_2 . To determine the IC_{50} s of the nine compounds, the compound concentrations were 1:1 serially diluted and added to the reaction solution before the reaction started. The reactions were started by the addition of 2 mM pNPP at 25°C , and the resulting increase in absorbance at 400 nm was measured using an ELx808 absorbance microplate reader (BioTek, Winooski, VT, USA). The IC_{50} s of the nine compounds were calculated from the linear slope of each reaction.

3.4. Casein Assay

Malachite green solution was used to monitor phosphate release from PP2C upon catalyzing a dephosphorylation reaction. The malachite green solution was prepared according to published methods [52,53] with some modification. First, 0.15 g malachite green was dissolved in 75 mL deionized water, and 2.5 g $(\text{NH}_4)_6\text{Mo}_7\text{O}_{24}\cdot 4\text{H}_2\text{O}$ was dissolved in 25 mL 4 M HCl. Then, the two solutions were mixed together and centrifuged at 1000 g for 10 min to remove precipitates. The supernatant from this solution was collected and used for the assay. Standard assays were performed in a volume of 100 μL containing 0.2 μg phosphatases in a buffer consisting of 10 mM Tris-Cl, pH 8.5; 50 mM NaCl; 1 mM DTT; and 2 mM MnCl_2 . To determine the catalytic constants for casein, the casein concentration was varied from 0.1 to 10 μM . From the linear slope of each reaction, the kinetic parameters K_m and V_{max} were calculated by nonlinear hyperbolic fitting using the GraphPad Prism 4 program (5.02, GraphPad Software Inc. La Jolla, CA, USA, 2009). To determine the IC_{50} s of the nine compounds, the compounds were 1:1 serially diluted and added to the reaction solution before the reaction started. The reactions were started by the addition of 40 μM casein. After a 10-min incubation at 25°C , each reaction was stopped by the addition of 50 μL 4.7 M HCl. The phosphate released from the dephosphorylation reaction was quantified colorimetrically using 100 μL of malachite green solution. The absorbance of the solution at 630 nm was measured using an ELx808 absorbance microplate reader (BioTek, Winooski, VT, USA). The IC_{50} s of the nine compounds were calculated from the measured optical density values.

3.5. tPphA Cross-Linking Reaction

tPphA glutardialdehyde cross-linking was performed as previously described [5] with some modifications. The cross-linking reaction was performed in a solution composed of 1 mM Tris-HCl, pH 7.4; 2.5 mM CaCl₂; 110 mM NaCl; 0.05 mM EDTA; and 0.08% (*w/w*) glutardialdehyde. After a 60 min incubation at 4 °C, tPphA and the cross-linked products were visualized by immunoblot analysis. DTSSP (3,3'-dithiobis [sulfosuccinimidylpropionate]) (Thermo Scientific Pierce, Rockford, IL, USA) was also used to cross-link tPphA. The cross-linking reaction was performed according to the manufacturer's instructions. The cross-linking solution was composed of 0.1 M phosphate, pH 7.2; 0.15 M NaCl; and 5 mM DTSSP. After a 2 h incubation at 4 °C, the reaction was stopped by the addition of 50mM Tris-HCl, pH 7.5. Subsequently, tPphA and the cross-linked products were mixed with SDS-PAGE loading buffer without DTT and visualized by immunoblot analysis. To break the disulfide bonds formed by DTSSP, the cross-linking products were mixed with SDS-PAGE loading buffer with DTT and visualized by immunoblot analysis.

3.6. Size Exclusion Chromatography

A total of 450 µg tPphA was incubated in 200 µL glutardialdehyde cross-linking solution under the same conditions described in the tPphA cross-linking reaction section above. After a 60 min incubation at 4 °C, the cross-linking solution was centrifuged at 14,000 rpm for 1 min to remove any aggregates from the solution. Following this, 200 µL of the solution was loaded onto a Superdex 200 10/300 GL column (GE). Size exclusion chromatography was conducted at a flow rate of 0.5 mL/min at 8 °C with a run time of 40 min. The cross-linking products were eluted using a buffer composed of 10 mM Tris-Cl, pH 7.4, and 150 mM NaCl and then filtered through a 0.02 µm filter. Elution fractions of 0.5 mL were collected. Finally, 50 µL from each elution fraction was used to test enzyme activity towards pNPP.

Acknowledgments: This work was supported by the National Natural Science Foundation of China under grant (NO. 31500637), the Drug Discovery Found of Jilin Province under grant (NO. 20150311057YY), the Natural Science Foundation of Jilin Province of China under grant (NO. 20160101343JC) and the Fundamental Research Funds for the Central Universities under grant (NO. 2412015KJ018). We thank the staff of BL18U beamline at the National Center for Protein Sciences Shanghai and the Shanghai Synchrotron Radiation Facility, Shanghai, People's Republic of China, for assistance during data collection. We also thank Zhengqiang Li and Shuai Li at Key Laboratory for Molecular Enzymology and Engineering of Ministry of Education, Jilin University, for their supports in initial protein crystal data collection.

Author Contributions: Yunlong Si and Ye Yuan participated in protein overexpression and solving tPphA structures. Yue Wang, Jin Gao, Yanbo Hu and Shiqiong Feng participated in pNPP assay, casein assay, chemical cross-linking and gel filtraion. Jiyong Su conceived of the study, participated in its design and coordination, and helped to draft the manuscript. All authors read and approved the final manuscript.

Conflicts of Interest: The authors declare no conflict of interest.

References

1. Fiscella, M.; Zhang, H.; Fan, S.; Sakaguchi, K.; Shen, S.; Mercer, W.E.; Woude, G.F.V.; O'Connor, P.M.; Appella, E. Wip1, a novel human protein phosphatase that is induced in response to ionizing radiation in a p53-dependent manner. *PNAS* **1997**, *94*, 6048–6053. [[CrossRef](#)] [[PubMed](#)]
2. Schweighofer, A.; Hirt, H.; Meskiene, I. Plant PP2C phosphatases: emerging functions in stress signaling. *Trends Plant Sci.* **2004**, *9*, 236–243. [[CrossRef](#)] [[PubMed](#)]
3. Arino, J.; Casamayor, A.; Gonzalez, A. Type 2C protein phosphatases in fungi. *Eukaryot. cell* **2011**, *10*, 21–33. [[CrossRef](#)] [[PubMed](#)]
4. Irmler, A.; Forchhammer, K. A PP2C-type phosphatase dephosphorylates the PII signaling protein in the cyanobacterium *Synechocystis* PCC 6803. *PNAS* **2001**, *98*, 12978–12983. [[CrossRef](#)] [[PubMed](#)]
5. Su, J.; Forchhammer, K. Determinants for substrate specificity of the bacterial PP2C protein phosphatase tPphA from *Thermosynechococcus elongatus*. *FEBS J.* **2013**, *280*, 694–707. [[CrossRef](#)] [[PubMed](#)]

6. Melcher, K.; Ng, L.M.; Zhou, X.E.; Soon, F.F.; Xu, Y.; Suino-Powell, K.M.; Park, S.Y.; Weiner, J.J.; Fujii, H.; Chinnusamy, V.; *et al.* A gate-latch-lock mechanism for hormone signalling by abscisic acid receptors. *Nature* **2009**, *462*, 602–608. [[CrossRef](#)] [[PubMed](#)]
7. Pullen, K.E.; Ng, H.L.; Sung, P.Y.; Good, M.C.; Smith, S.M.; Alber, T. An alternate conformation and a third metal in PstP/Ppp, the *M. tuberculosis* PP2C-Family Ser/Thr protein phosphatase. *Structure* **2004**, *12*, 1947–1954. [[CrossRef](#)] [[PubMed](#)]
8. Wehenkel, A.; Bellinzoni, M.; Schaeffer, F.; Villarino, A.; Alzari, P.M. Structural and binding studies of the three-metal center in two mycobacterial PPM Ser/Thr protein phosphatases. *J. Mol. Biol.* **2007**, *374*, 890–898. [[CrossRef](#)] [[PubMed](#)]
9. Rantanen, M.K.; Lehtio, L.; Rajagopal, L.; Rubens, C.E.; Goldman, A. Structure of Streptococcus agalactiae serine/threonine phosphatase. The subdomain conformation is coupled to the binding of a third metal ion. *FEBS J.* **2007**, *274*, 3128–3137. [[CrossRef](#)] [[PubMed](#)]
10. Bellinzoni, M.; Wehenkel, A.; Shepard, W.; Alzari, P.M. Insights into the catalytic mechanism of PPM Ser/Thr phosphatases from the atomic resolution structures of a mycobacterial enzyme. *Structure* **2007**, *15*, 863–872. [[CrossRef](#)] [[PubMed](#)]
11. Schlicker, C.; Fokina, O.; Kloft, N.; Grune, T.; Becker, S.; Sheldrick, G.M.; Forchhammer, K. Structural analysis of the PP2C phosphatase tPphA from *Thermosynechococcus elongatus*: A flexible flap subdomain controls access to the catalytic site. *J. Mol. Biol.* **2008**, *376*, 570–581. [[CrossRef](#)] [[PubMed](#)]
12. Su, J.; Schlicker, C.; Forchhammer, K. A third metal is required for catalytic activity of the signal-transducing protein phosphatase M tPphA. *J. Boil. Chem.* **2011**, *286*, 13481–13488. [[CrossRef](#)] [[PubMed](#)]
13. Gilmartin, A.G.; Faitg, T.H.; Richter, M.; Groy, A.; Seefeld, M.A.; Darcy, M.G.; Peng, X.; Federowicz, K.; Yang, J.; Zhang, S.Y.; *et al.* Allosteric Wip1 phosphatase inhibition through flap-subdomain interaction. *Nat. Chem. Biol.* **2014**, *10*, 181–187. [[CrossRef](#)] [[PubMed](#)]
14. Hayashi, R.; Tanoue, K.; Durell, S.R.; Chatterjee, D.K.; Jenkins, L.M.; Appella, D.H.; Appella, E. Optimization of a cyclic peptide inhibitor of Ser/Thr phosphatase PPM1D (Wip1). *Biochemistry* **2011**, *50*, 4537–4549. [[CrossRef](#)] [[PubMed](#)]
15. Lu, X.; Nguyen, T.A.; Moon, S.H.; Darlington, Y.; Sommer, M.; Donehower, L.A. The type 2C phosphatase Wip1: An oncogenic regulator of tumor suppressor and DNA damage response pathways. *Cancer Metastasis Rev.* **2008**, *27*, 123–135. [[CrossRef](#)] [[PubMed](#)]
16. Lowe, J.; Cha, H.; Lee, M.O.; Mazur, S.J.; Appella, E.; Fornace, A.J., Jr. Regulation of the Wip1 phosphatase and its effects on the stress response. *Front. Biosci.* **2012**, *17*, 1480–1498. [[CrossRef](#)]
17. Zhu, Y.H.; Bulavin, D.V. Wip1-dependent signaling pathways in health and diseases. *Prog. Mol. Biol. Transl. Sci.* **2012**, *106*, 307–325. [[PubMed](#)]
18. Cao, M.; Liu, X.; Zhang, Y.; Xue, X.; Zhou, X.E.; Melcher, K.; Gao, P.; Wang, F.; Zeng, L.; Zhao, Y.; *et al.* An ABA-mimicking ligand that reduces water loss and promotes drought resistance in plants. *Cell Res.* **2013**, *23*, 1043–1054. [[CrossRef](#)] [[PubMed](#)]
19. Leung, J.; Merlot, S.; Giraudat, J. The Arabidopsis ABSCISIC ACID-INSENSITIVE2 (ABI2) and ABI1 genes encode homologous protein phosphatases 2C involved in abscisic acid signal transduction. *Plant Cell* **1997**, *9*, 759–771. [[CrossRef](#)] [[PubMed](#)]
20. Leube, M.P.; Grill, E.; Amrhein, N. ABI1 of Arabidopsis is a protein serine/threonine phosphatase highly regulated by the proton and magnesium ion concentration. *FEBS Lett.* **1998**, *424*, 100–104. [[CrossRef](#)]
21. Gosti, F.; Beaudoin, N.; Serizet, C.; Webb, A.A.; Vartanian, N.; Giraudat, J. ABI1 protein phosphatase 2C is a negative regulator of abscisic acid signaling. *Plant Cell* **1999**, *11*, 1897–1910. [[CrossRef](#)] [[PubMed](#)]
22. Vlad, F.; Rubio, S.; Rodrigues, A.; Sirichandra, C.; Belin, C.; Robert, N.; Leung, J.; Rodriguez, P.L.; Lauriere, C.; Merlot, S. Protein phosphatases 2C regulate the activation of the Snf1-related kinase OST1 by abscisic acid in Arabidopsis. *Plant Cell* **2009**, *21*, 3170–3184. [[CrossRef](#)] [[PubMed](#)]
23. Aburai, N.; Yoshida, M.; Ohnishi, M.; Kimura, K. Sanguinarine as a potent and specific inhibitor of protein phosphatase 2C *in vitro* and induces apoptosis via phosphorylation of p38 in HL60 cells. *Biosci. Biotechnol. Biochem.* **2010**, *74*, 548–552. [[CrossRef](#)] [[PubMed](#)]
24. Weerasinghe, P.; Hallock, S.; Brown, R.E.; Loose, D.S.; Buja, L.M. A model for cardiomyocyte cell death: Insights into mechanisms of oncosis. *Exp. Mol. Pathol.* **2013**, *94*, 289–300. [[CrossRef](#)] [[PubMed](#)]

25. Adhami, V.M.; Aziz, M.H.; Mukhtar, H.; Ahmad, N. Activation of prodeath Bcl-2 family proteins and mitochondrial apoptosis pathway by sanguinarine in immortalized human HaCaT keratinocytes. *Clin. Cancer Res.* **2003**, *9*, 3176–3182.
26. Sun, M.; Lou, W.; Chun, J.Y.; Cho, D.S.; Nadiminty, N.; Evans, C.P.; Chen, J.; Yue, J.; Zhou, Q.; Gao, A.C. Sanguinarine suppresses prostate tumor growth and inhibits survivin expression. *Genes Cancer* **2010**, *1*, 283–292. [[CrossRef](#)] [[PubMed](#)]
27. Holy, J.; Lamont, G.; Perkins, E. Disruption of nucleocytoplasmic trafficking of cyclin D1 and topoisomerase II by sanguinarine. *BMC Cell Boil.* **2006**, *7*, 13. [[CrossRef](#)] [[PubMed](#)]
28. Malikova, J.; Zdarilova, A.; Hlobilkova, A.; Ulrichova, J. The effect of chelerythrine on cell growth, apoptosis, and cell cycle in human normal and cancer cells in comparison with sanguinarine. *Cell Boil. Toxicol.* **2006**, *22*, 439–453. [[CrossRef](#)] [[PubMed](#)]
29. Pica, F.; Balestrieri, E.; Serafino, A.; Sorrentino, R.; Gaziano, R.; Moroni, G.; Moroni, N.; Palmieri, G.; Mattei, M.; Garaci, E. Antitumor effects of the benzophenanthridine alkaloid sanguinarine in a rat syngeneic model of colorectal cancer. *Anti-Cancer Drugs* **2012**, *23*, 32–42. [[CrossRef](#)] [[PubMed](#)]
30. Klumpp, S.; Selke, D.; Fischer, D.; Baumann, A.; Muller, F.; Thanos, S. Protein phosphatase type-2C isozymes present in vertebrate retinae: purification, characterization, and localization in photoreceptors. *J. Neurosci. Res.* **1998**, *51*, 328–338. [[CrossRef](#)]
31. Klumpp, S.; Selke, D.; Hermesmeier, J. Protein phosphatase type 2C active at physiological Mg^{2+} : Stimulation by unsaturated fatty acids. *FEBS Lett.* **1998**, *437*, 229–232. [[CrossRef](#)]
32. Wang, Y.; Santini, F.; Qin, K.; Huang, C.Y. A Mg^{2+} -dependent, Ca^{2+} -inhibitable serine/threonine protein phosphatase from bovine brain. *J. Biol. Chem.* **1995**, *270*, 25607–25612. [[CrossRef](#)] [[PubMed](#)]
33. Signorile, A.; Sardanelli, A.M.; Nuzzi, R.; Papa, S. Serine (threonine) phosphatase(s) acting on cAMP-dependent phosphoproteins in mammalian mitochondria. *FEBS Lett.* **2002**, *512*, 91–94. [[CrossRef](#)]
34. Mukhopadhyay, S.; Kapatral, V.; Xu, W.; Chakrabarty, A.M. Characterization of a Hank's type serine/threonine kinase and serine/threonine phosphoprotein phosphatase in *Pseudomonas aeruginosa*. *J. Bacteriol.* **1999**, *181*, 6615–6622. [[PubMed](#)]
35. Takezawa, D. Characterization of a novel plant PP2C-like protein Ser/Thr phosphatase as a calmodulin-binding protein. *J. Biol. Chem.* **2003**, *278*, 38076–38083. [[CrossRef](#)] [[PubMed](#)]
36. Bevilaqua, L.R.; Cammarota, M.; Dickson, P.W.; Sim, A.T.; Dunkley, P.R. Role of protein phosphatase 2C from bovine adrenal chromaffin cells in the dephosphorylation of phospho-serine 40 tyrosine hydroxylase. *J. Neurochem.* **2003**, *85*, 1368–1373. [[CrossRef](#)] [[PubMed](#)]
37. Sierecki, E.; Newton, A.C. Biochemical characterization of the phosphatase domain of the tumor suppressor PH domain leucine-rich repeat protein phosphatase. *Biochemistry* **2014**, *53*, 3971–3981. [[CrossRef](#)] [[PubMed](#)]
38. Sugiura, T.; Noguchi, Y. Substrate-dependent metal preference of PPM1H, a cancer-associated protein phosphatase 2C: Comparison with other family members. *Biometals* **2009**, *22*, 469–477. [[CrossRef](#)] [[PubMed](#)]
39. Marley, A.E.; Sullivan, J.E.; Carling, D.; Abbott, W.M.; Smith, G.J.; Taylor, I.W.; Carey, F.; Beri, R.K. Biochemical characterization and deletion analysis of recombinant human protein phosphatase 2C alpha. *Biochem. J.* **1996**, *320*, 801–806. [[CrossRef](#)] [[PubMed](#)]
40. Schenk, G.; Elliott, T.W.; Leung, E.; Carrington, L.E.; Mitic, N.; Gahan, L.R.; Guddat, L.W. Crystal structures of a purple acid phosphatase, representing different steps of this enzyme's catalytic cycle. *BMC Struct. Boil.* **2008**, *8*, 6. [[CrossRef](#)] [[PubMed](#)]
41. Wang, W.; Cho, H.S.; Kim, R.; Jancarik, J.; Yokota, H.; Nguyen, H.H.; Grigoriev, I.V.; Wemmer, D.E.; Kim, S.H. Structural characterization of the reaction pathway in phosphoserine phosphatase: Crystallographic "snapshots" of intermediate states. *J. Mol. Boil.* **2002**, *319*, 421–431. [[CrossRef](#)]
42. Lopez-Gallego, F.; Guisan, J.M.; Betancor, L. Glutaraldehyde-mediated protein immobilization. *Methods Mol. Boil.* **2013**, *1051*, 33–41.
43. Kabsch, W. XDS. *Acta Crystallogr. D Biol. Crystallogr.* **2010**, *66*, 125–132. [[CrossRef](#)] [[PubMed](#)]
44. Evans, P.R.; Murshudov, G.N. How good are my data and what is the resolution? *Acta Crystallogr. D Biol. Crystallogr.* **2013**, *69*, 1204–1214. [[CrossRef](#)] [[PubMed](#)]
45. Potterton, E.; Briggs, P.; Turkenburg, M.; Dodson, E. A graphical user interface to the CCP4 program suite. *Acta Crystallogr. D Biol. Crystallogr.* **2003**, *59*, 1131–1137. [[CrossRef](#)] [[PubMed](#)]
46. McCoy, A.J.; Grosse-Kunstleve, R.W.; Adams, P.D.; Winn, M.D.; Storoni, L.C.; Read, R.J. Phaser crystallographic software. *J. Appl. Crystallogr.* **2007**, *40*, 658–674. [[CrossRef](#)] [[PubMed](#)]

47. Adams, P.D.; Afonine, P.V.; Bunkoczi, G.; Chen, V.B.; Davis, I.W.; Echols, N.; Headd, J.J.; Hung, L.W.; Kapral, G.J.; Grosse-Kunstleve, R.W.; *et al.* PHENIX: A comprehensive Python-based system for macromolecular structure solution. *Acta Crystallogr. D Biol. Crystallogr.* **2010**, *66*, 213–221. [[CrossRef](#)] [[PubMed](#)]
48. Chen, V.B.; Arendall, W.B., 3rd; Headd, J.J.; Keedy, D.A.; Immormino, R.M.; Kapral, G.J.; Murray, L.W.; Richardson, J.S.; Richardson, D.C. MolProbity: All-atom structure validation for macromolecular crystallography. *Acta Crystallogr. D Biol. Crystallogr.* **2010**, *66*, 12–21. [[CrossRef](#)] [[PubMed](#)]
49. Davis, I.W.; Leaver-Fay, A.; Chen, V.B.; Block, J.N.; Kapral, G.J.; Wang, X.; Murray, L.W.; Arendall, W.B., 3rd; Snoeyink, J.; Richardson, J.S.; *et al.* MolProbity: All-atom contacts and structure validation for proteins and nucleic acids. *Nucleic Acids Res.* **2007**, *35*, W375–W383. [[CrossRef](#)] [[PubMed](#)]
50. The PyMOL Molecular Graphics System, Version 1.7.2. Schrödinger LLC, 2015. Available online: www.pymol.org (accessed on 25 April 2016).
51. Emsley, P.; Lohkamp, B.; Scott, W.G.; Cowtan, K. Features and development of Coot. *Acta Crystallogr. D Biol. Crystallogr.* **2010**, *66*, 486–501. [[CrossRef](#)] [[PubMed](#)]
52. Van Veldhoven, P.P.; Mannaerts, G.P. Inorganic and organic phosphate measurements in the nanomolar range. *Anal. Biochem.* **1987**, *161*, 45–48. [[CrossRef](#)]
53. Ekman, P.; Jager, O. Quantification of subnanomolar amounts of phosphate bound to seryl and threonyl residues in phosphoproteins using alkaline hydrolysis and malachite green. *Anal. Biochem.* **1993**, *214*, 138–141. [[CrossRef](#)] [[PubMed](#)]



© 2016 by the authors; licensee MDPI, Basel, Switzerland. This article is an open access article distributed under the terms and conditions of the Creative Commons Attribution (CC-BY) license (<http://creativecommons.org/licenses/by/4.0/>).